Structure
Article

Global Conformational Changes of Ribosome Observed by Normal Mode Fitting for 3D Cryo-EM Structures

Atsushi Matsumoto[1,2,*] and Hisashi Ishida[1,2]
[1]Center for Computational Science and Engineering
[2]Quantum Beam Science Directorate
Japan Atomic Energy Agency, 8-1-7 Umemidai, Kizugawa, Kyoto 619-0215, Japan
*Correspondence: matsumoto.atsushi@jaea.go.jp
DOI 10.1016/j.str.2009.09.017

SUMMARY

Many three-dimensional density maps of 70S ribosome at various functional states are available now in the Electron Microscopy DataBank at EBI. We used our new flexible-fitting approach to systematically analyze these maps to reveal the global conformational differences between the EM structures. Large-scale ratchet-like deformations were observed in an EM structure of the initiation complex and in some EM structures bound with EFG, RF3, and RRF. In most of them, the L1 stalk, which interacts with the tRNA molecule at the E site of ribosome and is considered to be involved in the release of the tRNA, was in "the blocking state" for the E-tRNA. Furthermore, we found that the EM structures bound with EFG or RRF were aligned in the conformational space, suggesting that the large-scale conformational changes of the 70S ribosome bound with these factors occur along a specific pathway in a concerted manner.

INTRODUCTION

Ribosome is a huge macromolecular complex responsible for protein synthesis in all organisms. In prokaryotes, the large 50S subunit and small 30S subunit form the 70S ribosome. The large subunit consists of a 23S rRNA, a 5S sRNA, and 34 proteins, and the small subunit consists of a 16S rRNA and 21 proteins.

There are four essential steps during protein synthesis in ribosome; initiation, elongation, termination, and recycling. In the initiation step, the two subunits come together and bind to mRNA and form an initiation complex of the 70S ribosome. In the elongation step, ribosome synthesizes proteins by translating the base sequence information on mRNA to the amino-acid sequence. In the termination step, protein synthesis is terminated, and the newly synthesized peptide chain is released. Finally, in the recycling step, ribosome dissociates into two subunits for a new cycle of protein synthesis. Recent progress in cryo–electron microscopy (EM) has made it possible to capture three-dimensional structures of ribosome at each of these different steps. From the comparison of these EM structures, functionally important conformational changes have been identified. Among these changes, the ratchet-like rotational motion of the 30S subunit relative to the 50S subunit during the translocation process in the elongation step (Frank and Agrawal, 2000) is one of the most important global motions observed in ribosome. The ratchet-like motion was later observed by the normal mode calculations of the elastic network model (Tama et al., 2003; Wang et al., 2004).

We were inspired by these experimental and computational results and consequently started conformational analyses of the EM structures ourselves. We analyzed 44 EM structures of prokaryotes ribosome (*Escherichia coli* and *Thermus Thermophilus*) using a new flexible-fitting approach. These structures are available from the Electron Microscopy DataBank (EMDB) at the European Bioinformatics Institute (EBI). Because of the low resolution nature of the EM structures, it would be difficult to examine the local structural differences. Instead, we concentrated on the global conformational differences between the EM structures. We were especially interested in the ratchet-like global motion, and our results have revealed how this motion is involved in coordinating the conformational changes of ribosome during protein synthesis.

RESULTS AND DISCUSSION

Fitting the PDB Structure into EM Structures

Table 1 lists the 44 EM structures (Agrawal et al., 2004; Allen et al., 2005; Barat et al., 2007; Connell et al., 2007; Diaconu et al., 2005; Gabashvili et al., 2000; Gao et al., 2007, 2005; Gilbert et al., 2004; Gillet et al., 2007; Halic et al., 2006; Kaur et al., 2006; Klaholz et al., 2004, 2003; Konevega et al., 2007; Marzi et al., 2007; Mitra et al., 2005; Myasnikov et al., 2005; Rawat et al., 2006, 2003; Schaffitzel et al., 2006; Stark et al., 2002; Valle et al., 2002, 2003a, 2003b, 2003c) of the 70S ribosome that we studied here. Each row shows the EM-ID, the resolution, the voxel size, the initial and final fitting scores, and the names of the bound molecules. The voxel size was given as an experimental value in the EMDB and the references. The initial scores in Table 1 show the fitting scores for the PDB structure (PDBID: 1YL3 and 1YL4; Jenner et al., 2005; see also Experimental Procedures) fitted into the EM structures. Our scoring function was defined as a ratio of the number of atoms overlapped with the EM structure, which we regarded as a continuum, to the total number of atoms. For this scoring function, the surface (or the boundary) of the EM structure must be defined, and we defined it so that the volume

Table 1. List of EM structures and their fitting scores

EM-ID	Resolution (Å)	Voxel Size (Å)	Initial Score	Final Score	Bound Molecules[a]
1003[b]	11.5	2.93	0.867	0.875	P
1004[c]	16	2.25	0.735	0.741	P, A, EF-Tu
1005[d]	21	2.40	0.696	0.700	P, RF2
1006[e]	11.3	2.82	0.832	0.839	E, P
1007[e]	12.9	2.82	0.842	0.849	E, P, RF2
1008[e]	10.9	2.82	0.839	0.847	E, P, RF2
1045[f]	16.8	2.69	0.852	0.859	P, A, EF-Tu
1055[g]	10.25	2.82	0.806	0.813	P, A, EF-Tu
1056[g]	10.25	2.82	0.813	0.821	E, P, A
1064[h]	23.8	2.40	0.666	0.669	P, RF3
1065[h]	24.7	2.40	0.604	0.626	P, RF3
1068[i]	13.4	3.33	0.802	0.808	—
1070[i]	13.4	3.33	0.829	0.834	P, E
1071[i]	13.2	3.33	0.753	0.757	P, E
1072[i]	16	3.33	0.800	0.804	P, E
1077[j]	12	2.82	0.825	0.836	RRF
1110[k]	18[l]	3.20	0.725	0.745	EFG
1122[m]	14.5	2.82	0.823	0.830	P, tmRNA
1128[n]	14.1	2.82	0.761	0.795	P/E, RRF
1143[o]	14.9	3.59	0.853	0.863	E, P, A, SecYEG
1172[p]	14.3	3 (2.40)	0.297 (0.594)	—	P, IF2
1173[p]	13.1	3 (2.40)	0.321 (0.544)	—	P, IF2
1184[q]	12.8	2.82	0.837	0.843	E, P, RF1
1185[q]	14	2.82	0.815	0.820	E, P, RF1
1248[r]	13.8	2.82	0.819	0.832	P, IF1, 2, 3
1250[s]	15.5	3.81	0.757	0.762	E, P, A
1251[s]	20	3.81	0.750	0.758	E, P, A, SRP
1261[t]	9.5	1.23	0.801	0.806	P, SRP
1262[t]	10.7	1.23	0.850	0.855	P, TF
1263[t]	9.1	1.23	0.875	0.884	P
1302[u]	15.5	2.82	0.795	0.818	P/E, RF3
1310[v]	11.8	2.82	0.843	0.848	E, P, SmpB
1311[w]	13.6	2.82	0.800	0.810	P, tmRNA
1312[v]	13.1	2.82	0.827	0.835	P, tmRNA
1315[x]	7.3	1.26	0.822	0.864	P/E, EFG
1323[y]	22	2.80	0.744	0.753	P, A
1324[y]	17	2.80	0.767	0.775	P
1362[z]	12.5	2.82	0.810	0.816	P, EFG
1363[z]	10.9	2.82	0.770	0.800	P/E, EFG
1365[z]	11.75	2.82	0.783	0.800	P/E, EFG
1366[z]	12.8	2.82	0.814	0.822	P, EFG
1370[aa]	15.3	2.76	0.803	0.822	P/E, RRF
1391[bb]	10[cc]	3 (2.40)	0.359 (0.736)	0.740	S15mRNA
1395[g]	12.8	2.82	0.829	0.835	P, IF1, 2, 3

The resolutions are based on Fourier shell correlation at 0.5 cut-off unless otherwise noted.

[a] Only tRNAs and characteristic molecules are shown. E, P, A, and P/E refer to E-tRNA, P-tRNA, A-tRNA, and P/E-tRNA, respectively.

[b] Gabashvili et al. (2000).

[c] Stark et al. (2002).

[d] Klaholz et al. (2003).

[e] Rawat et al. (2003).

[f] Valle et al. (2002).

[g] Valle et al. (2003b).

[h] Klaholz et al. (2004).

[i] Gilbert et al. (2004).

[j] Agrawal et al. (2004).

[k] Diaconu et al. (2005).

[l] The resolution is based on FSC at 5σ cut-off.

[m] Valle et al. (2003a).

[n] Gao et al. (2005).

[o] Mitra et al. (2005).

[p] Myasnikov et al. (2005).

[q] Rawat et al. (2006).

[r] Allen et al. (2005).

[s] Schaffitzel et al. (2006).

[t] Halic et al. (2006).

[u] Gao et al. (2007).

[v] Gillet et al. (2007).

[w] Kaur et al. (2006).

[x] Connell et al. (2007).

[y] Konevega et al. (2007).

[z] Valle et al. (2003c).

[aa] Barat et al. (2007).

[bb] Marzi et al. (2007).

[cc] The resolution is based on FSC at 0.14 cut-off.

of the EM structure was equivalent to that of the PDB structure (see also Experimental Procedures). This simple scoring function was used mainly for the fast calculations.

Most of the scores were greater than 0.75, suggesting that the PDB structure fitted well. However, the fitting scores were not as good for EMD-1172, -1173, and -1391. By visually comparing these EM structures with the PDB structure, we found that the size of the outer forms of these EM structures was much larger than that of the PDB structure. This finding suggests that the voxel size given as the experimental value was too large. To verify this, we decreased the voxel size at intervals of 0.05 Å and checked whether the fitting had improved. Indeed, the fitting scores for the three EM structures had improved. Although the improvement for EMD-1391 was drastic, the scores for EMD-1172 and -1173 were still low. Thus, we excluded these EM structures (EMD-1172 and -1173) from any further analysis. The optimum voxel sizes and the improved scores are shown in parentheses (Table 1).

Building a Library of Deformed Atomic Structures

In the usual flexible-fitting approach for building an atomic model from a 3D-EM map (Tama et al., 2004a, 2004b; Trabuco et al., 2008), the atomic structure is iteratively deformed so that the fitting to the EM structure is improved. In other words, the best-fitting atomic structure is tailor-made for each EM structure. In this study, we took a different approach (Figure 1). First, we prepared many different deformed atomic structures. Then, we identified the atomic structure that best-fitted each EM structure. In other words, we built a library of deformed atomic structures and then selected the best-fitting atomic structure for each EM structure from our library of ready-made deformed atomic structures. In the tailor-made approach, time-consuming calculation for deforming the atomic structure must be performed for

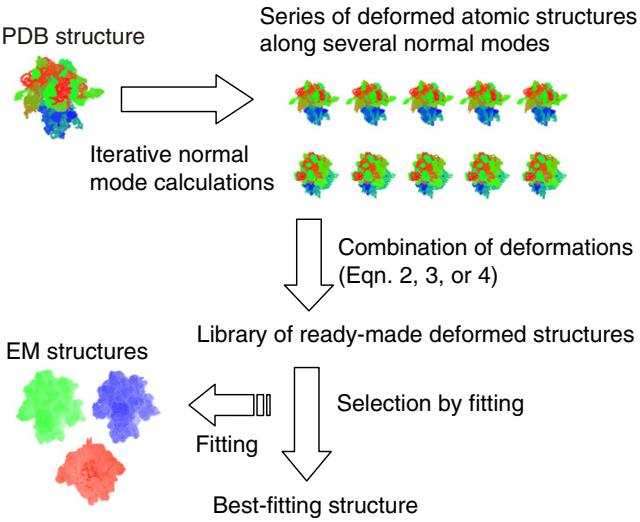

Figure 1. An Overview of Our Ready-Made Flexible-Fitting Approach to Build Atomic Structures from EM Structures

The molecular images were generated by program VMD (Humphrey et al., 1996).

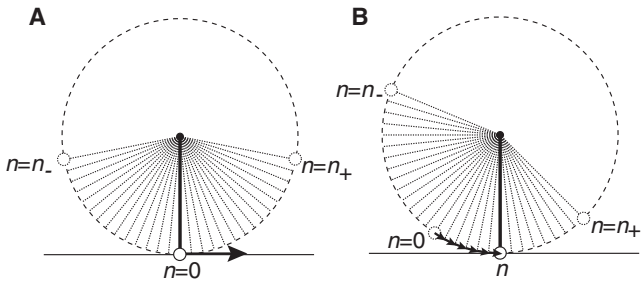

Figure 2. The Limitation of Deformation along a Normal Mode Vector and the Effect of the Iterative Normal Mode Calculations Demonstrated by a Pendulum

(A) If the pendulum is moved along the normal mode vector (shown by an arrow) too far, it deviates from the low-energy path (dashed line) which it should follow. This results in a large increase in the energy due to the extension of the string (thick solid line).

(B) If small movements along the normal mode vectors are repeated, the pendulum moves approximately along the low-energy path.

each EM structure. On the other hand, in our ready-made approach, once the library is built, only the rigid-body fitting calculations, which require much less computational time, are necessary. Thus, when we study many EM structures of the same target, the latter approach can save computational time. Also, the comparison of the EM structures is straightforward, as is shown later.

To build deformed atomic structures, we employed normal mode analysis. In the normal mode analysis, molecular deformation can be described by a sum of normal modes as follows:

$$\mathbf{r} - \mathbf{r}_0 = \sum_k \alpha_k \mathbf{v}_0^k, \quad (1)$$

where $\mathbf{r}$ and $\mathbf{r}_0$ are the vectors describing the deformed and energy-minimized atomic structures, respectively, $\mathbf{v}_0{}^k$ is the kth normal mode vector for the structure $\mathbf{r}_0$, and α_k is the coefficient. This equation is a good approximation only when the deformation (α_k) is small. When the deformation is large, the molecule does not deform along the low-energy path as it should (Figure 2A). Miyashita et al. (2003) showed that atomic structures with large deformations along the low-energy path could be obtained by applying small deformations along the normal mode iteratively (Figure 2B). By this approach, we obtained a few series of deformed atomic structures $\mathbf{r}^k{}_n$ along the kth normal mode (see Experimental Procedures). Using the deformed atomic structures $\mathbf{r}^k{}_n$, we replaced Equation 1 with the following equation for larger molecular deformation:

$$\mathbf{r} - \mathbf{r}_0 = \sum_k (\mathbf{r}^k_{nk} - \mathbf{r}_0), \quad (2)$$

where $\mathbf{r}^k_{nk}$ is the n_k-th structure along the kth normal mode. Note that $\mathbf{r}$ in Equation 1 is determined by real numbers (α_1, α_2, α_3,...), whereas $\mathbf{r}$ in Equation 2 is determined by integers (n_1, n_2, n_3,...). We built each series of deformed atomic structures $\mathbf{r}^k{}_n$ at the interval of 0.1 Å in root-mean-square displacement (rmsd). The library of the ready-made deformed atomic structures $\mathbf{r}$ in Equation 2 is easily built once the deformed atomic structures $\mathbf{r}^k{}_n$ are obtained.

We built a series of deformed atomic structures $\mathbf{r}^k{}_n$ along the third, fifth, sixth, seventh, and ninth lowest frequency normal modes. This was the most time-consuming part in this study, and we needed to choose along which normal modes we should build the deformed structures. In choosing the normal modes, we first restricted our attention to the 10 lowest frequency modes, because in low-frequency normal modes, large structural fluctuations occur with a small amount of energy (see, for example, Matsumoto and Olson, 2002) and can be related to the molecular function. Then, from the 10 normal modes, we chose which modes to use on the basis of two points of view. First, the normal modes should be effective in increasing the fitting score. The deformation of the PDB structure is performed so that the fitting to the EM structures improves. It is best if the deformation along the normal mode is effective for as many EM structures as possible. Second, the normal mode motions should be global. As described in the Introduction, we were interested in the global conformational differences between the EM structures. Thus, the normal modes used in building the deformed atomic structures should show global motions. A detailed explanation of our choice of the normal modes is included in the Supplemental Data available online.

In Figures 3A–3C, the displacement vectors, which show the atomic movements, in the third, fifth, and sixth modes are shown. In Figure 3D, some of the deformed atomic structures $\mathbf{r}^k{}_n$ along the third, fifth, and sixth modes are shown. As is described in the Introduction, we were interested in the ratchet-like motion of the 70S ribosome and we observed it in the sixth lowest frequency mode by visually inspecting each normal mode (see also the Supplemental Movies).

As described above, each series of deformed atomic structures $\mathbf{r}^k{}_n$ was built at the interval of 0.1 Å in rmsd, and the rmsd of $\mathbf{r}^k{}_{n+10}$ from $\mathbf{r}^k{}_n$ was roughly 1 Å. However, it should be noted that the atomic movements were partly much larger than the

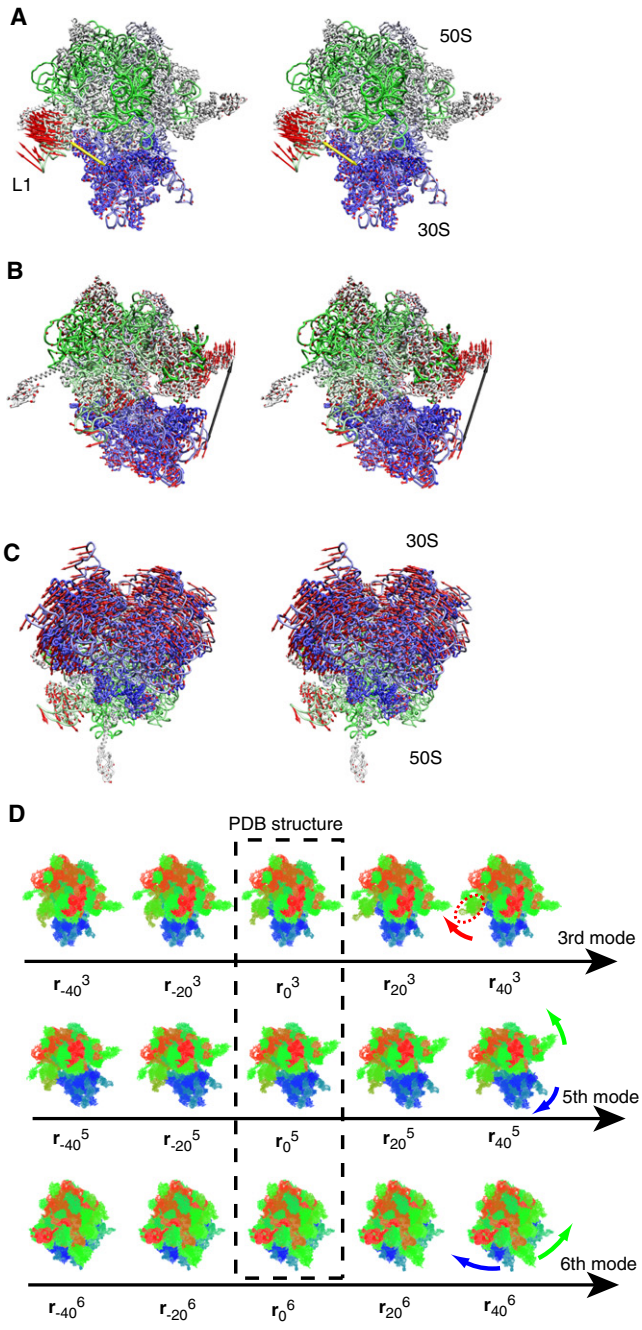

Figure 3. Displacement Vectors of the Cα and P Atoms

(A-C) Displacement vectors of the Cα and P atoms when the X-ray crystal structure is changed to the 50th deformed structure along the k th mode ($\mathbf{r}^k_{50}$), where $k = 3$ (A), $k = 5$ (B), and $k = 6$ (C), depicted with the backbone model of the PDB structure. The yellow (A) and black (B) arrows are drawn between Asn81 and Glu3089, and between Gly4303 and C7901, respectively. Although the root-mean-square displacements of the deformed structures ($\mathbf{r}^3_{50}$ $\mathbf{r}^5_{50}$, $\mathbf{r}^6_{50}$) from the PDB structure are all about 5 Å, the maximum displacements of the residues are 62 Å (A), 24 Å (B), and 24 Å (C), respectively.

(D) Atomic structures $\mathbf{r}^k_n$ deformed along the third, fifth, and sixth modes ($k = 3$, 5, and 6). The images were generated by a program VMD (Humphrey et al., 1996).

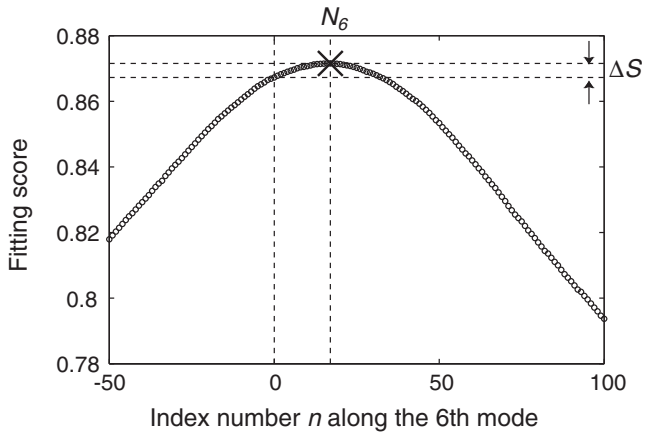

Figure 4. Fitting Scores of a Series of the Deformed Atomic Structures $\mathbf{r}^6_n$ along the Sixth Lowest Frequency (Ratchet-Like) Mode for EMD-1003 Are Plotted Against Index Number n

The maximum score is indicated by a cross.

rmsd value (see also the legend to Figure 3), because in low-frequency modes, the atomic movements are cooperative. For example, the distance between Asn81 and Glu3089 shown by a yellow arrow in Figure 3A and the distance between Gly4303 and C7901 shown by a black arrow in Figure 3B were extended by about 8 Å and 7.5 Å when the PDB structure $\mathbf{r}_0$ was deformed along the positive directions of the third mode and fifth mode by 1 Å in rmsd, respectively. In the sixth mode, the 30S subunit rotated with respect to the 50S subunit by about 1.4° when the rmsd was changed by 1 Å, which was calculated by a program called Dyndom3D (Poornam et al., 2009).

One-Dimensional Search: Ranking the Normal Modes

We have built a series of deformed atomic structures $\mathbf{r}^k_n$ along the third, fifth, sixth, seventh, and ninth lowest-frequency normal modes. Here, we searched each series of deformed atomic structures for the best-fitting structure for each EM structure to see which normal modes should be used for the summation in Equation 2, or for building the library. We especially wanted to use the normal modes that would yield the largest increase in the fitting score. We also considered the distribution of the best-fitting atomic structure along each normal mode; a wide distribution along a normal mode suggests that the motion described by the normal mode may be functionally important for the 70S ribosome.

The deformed atomic structures $\mathbf{r}^k_n$ along each of the five normal modes were fitted into each EM structure and the fitting scores were calculated. As an example, Figure 4 shows the fitting scores for the deformed atomic structures along the sixth lowest frequency (ratchet-like) mode into EMD-1003, a ribosome structure bound with formyl-methionyl initiator $tRNA^{fMet}$. We regarded the structure with the maximum score (shown by a cross in Figure 4) as the best-fitting atomic structure along this mode for EMD-1003. We defined N_k as the index number n of the best-fitting structure $\mathbf{r}^k_n$ and ΔS as the increase in the fitting score of the best-fitting structure with respect to that for the PDB structure ($n = 0$). In the same way, we identified the best-fitting atomic structure for each of the 42 EM structures

Table 2. The Average Values of ΔS and N_k and the Standard Deviation of N_k Obtained by the 1D Search for the 42 EM Structures

Mode number k	$< \Delta S > /10^{-3}$	$< N_k >$	STD(N_k)
3	1.74	8.7	14.5
5	3.48	15.4	6.8
6	5.83	20.3	14.5
7	0.60	5.4	4.9
9	1.30	9.6	13.7

along each of the five normal modes and obtained N_k and ΔS. The average values of ΔS and N_k and standard deviation of N_k for the 42 EM structures are summarized in Table 2. With respect to the increase in the fitting score, the sixth mode was the best mode to be used in Equation 2, followed by the fifth and the third modes. With respect to the distribution of the best-fitting structure (standard deviation of N_k), both the third and sixth modes were the best, followed by the ninth mode.

Table 2 also shows that the mean value of N_k is largest along the sixth mode, followed by the fifth mode. Interestingly, N_k values for the 42 EM structures along these two modes were all positive, suggesting that, compared with the PDB structure, all the EM structures were deformed in the direction of the vectors (not in the opposite direction) shown in Figures 3B and 3C. This may reflect the effect of the crystal packing. The PDB structure, which was determined by X-ray crystallography in the presence of $tRNA^{fMet}$, may be extremely deformed compared with the EM structures, which are considered to be obtained in a near-native environment.

Two-Dimensional Search

According to Equation 2, the deformed atomic structures are described by the sum of deformations along the selected normal modes. In this study, we used three normal modes at most for the summation in Equation 2. If we had used more normal modes, atomic structures with higher fitting scores would have been possible. However, we would have had to search the higher-dimensional space of the configuration, which, because of the increased number of candidates for the best-fitting structure, would have required a lot more computational time for the fitting calculations. Thus, we needed to restrict the number of normal modes used.

In the previous subsection, we found that the fifth and sixth modes yielded the most effective improvements in the fitting scores (Table 2). Thus, before using three normal modes, we considered it best to find the best-fitting atomic structures using these two normal modes, or in 2D space, and consider other normal modes later. In this way, we could reduce the number of candidates for the best-fitting structure, because the best-fitting structure in 3D space would not be very different from that obtained in 2D space.

From Equation 2, the atomic structures deformed along the fifth and sixth modes are described as follows:

$$\mathbf{r}(n_5, n_6) = \mathbf{r}_0 + \Delta\mathbf{r}^5_{n5} + \Delta\mathbf{r}^6_{n6}, \quad (3)$$

where $\Delta\mathbf{r}^k_{nk} (= \mathbf{r}^k_{nk} - \mathbf{r}_0)$ describes the deformation of the structure $\mathbf{r}^k_{nk}$ from the PDB structure $\mathbf{r}_0$.

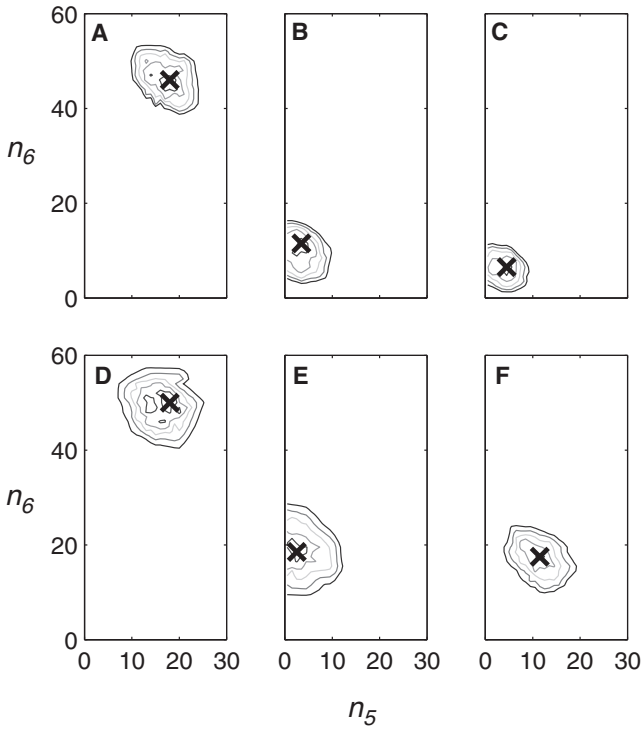

Figure 5. Contour Plots of the Fitting Scores Obtained by the Two-Dimensional Search for Six EM Structures

(A) EMD-1315 (resolution: 7.3 Å).
(B) EMD-1263 (9.1 Å).
(C) EMD-1261 (9.5 Å).
(D) EMD-1065 (24.7 Å).
(E) EMD-1064 (23.8 Å).
(F) EMD-1323 (22 Å).

The score for $\mathbf{r}(n_5, n_6)$ (Equation 3) is plotted at (n_5, n_6). The position of the highest score is indicated by a cross. The outermost contour runs through the points with scores smaller than the highest by 0.001 (0.1%).

We built many different atomic structures $\mathbf{r}$ (n_5, n_6) and calculated their fitting scores for each EM structure to identify the best-fitting atomic structure $\mathbf{r}(N_5^{(2)}, N_6^{(2)})$ in 2D space. The contour plots of the fitting scores for several EM structures are shown in Figure 5. Figures 5A–5C are the plots for the EM structures with the highest resolutions among the 42 EM structures (7.3, 9.1, and 9.5 Å, respectively), and Figures 5D–5F are the ones with the lowest resolutions (24.7, 23.8, and 22 Å, respectively). The regions encircled by the outermost contour in Figures 5A–5C tended to be smaller than those in the plots with larger resolutions (Figures 5D–5F). This finding suggests that the best-fitting atomic structures could be determined with more certainty from EM structures with higher resolutions. Although the resolution in the 3D-EM is determined in a completely different way (e.g., by using the Fourier shell correlation) from those in other experimental methods such as X-ray crystallography (Frank, 1996), this result suggests that the resolution in the 3D-EM is qualitatively consistent with the general idea of resolution; the details of the electron-density map become more distinctive as the resolution becomes higher. The result that the fitting scores tended to be higher for the EM structures with higher resolutions (Table 1) is also consistent with this idea.

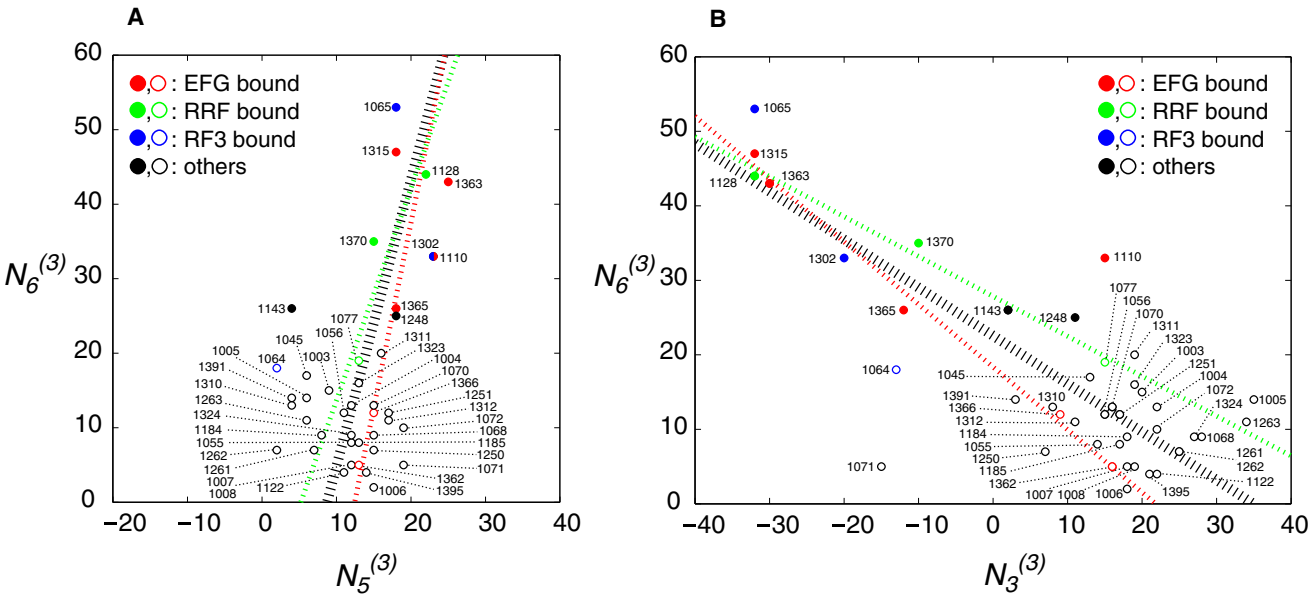

Figure 6. The Positions of the Best-Fitting Atomic Structures Obtained by the 3D Search

The black dotted line was drawn in such a way that the sum of squared distances from the line to the points for all structures was smallest. Similarly, the dotted red and green lines were drawn for the structures bound with EFG (except for EMD-1110) and RRF, respectively. They are projected on the plane defined by fifth and sixth modes (A), and on the plane defined by the 3rd and sixth modes (B). The EM-IDs are shown for all the structures. The best-fitting atomic structures for EM structures bound with EFG are shown by red circles, those with RRF by green, and those with RF3 by cyan. The others are shown by black circles. Solid circles indicate the structures with large ratchet-like deformations ($N_6^{(3)} \geq 25$).

Three-Dimensional Search

Similar to Equation 3, the atomic structures deformed along 3 normal modes (two of them are fifth and sixth modes) are described as follows:

$$\mathbf{r}(n_k, n_5, n_6) = \mathbf{r}_0 + \Delta\mathbf{r}_{nk}^k + \Delta\mathbf{r}_{n5}^5 + \Delta\mathbf{r}_{n6}^6. \quad (4)$$

However, searching the 3D space (n_k, n_5, n_6) for the best-fitting structure without any prior knowledge requires a lot of computational time. Thus, we first fixed the deformation along the fifth and sixth modes to that of the best-fitting structure $\mathbf{r}(N_5^{(2)}, N_6^{(2)})$ obtained by the 2D search and allowed the deformation only along the kth mode;

$$\mathbf{r}\left(n_k, N_5^{(2)}, N_6^{(2)}\right) = \mathbf{r}\left(N_5^{(2)}, N_6^{(2)}\right) + \Delta\mathbf{r}_{nk}. \quad (5)$$

We call this a quasi-3D search, but this is essentially the same as the 1D search, because only n_k is variable. Each series of atomic structures $\mathbf{r}(n_k, N_5^{(2)}, N_6^{(2)})$ was fitted into each EM structure and the best-fitting structure ($n_k = N_k'$) was identified. This search was performed along the third, seventh and ninth modes (k = 3, 7, or 9). The 1D search had already shown that the third mode was the most important among the third, seventh and ninth modes (Table 2). Thus, we could have done this search only along the third mode. However, we were not sure whether this ranking would change in this quasi-3D search because, in the 1D search, the increase in the fitting score was measured with respect to the PDB structure, but in this search, it was measured with respect to the best-fitting structure $\mathbf{r}(N_5^{(2)}, N_6^{(2)})$ obtained by the 2D search. Thus, we performed the quasi-3D search along all three of these normal modes.

In Table S2, the average values of N_k' and $\Delta S'$, the increase in the fitting score due to the deformation $\Delta\mathbf{r}_{Nk'}^k$ from $\mathbf{r}(N_5^{(2)}, N_6^{(2)})$, and the standard deviation of N_k' for the 42 EM structures are summarized. The conclusion drawn from this table is the same as that from Table 2; the third mode was the most important among the third, seventh and ninth modes. Thus, we concluded that the deformations along the third, fifth, and sixth modes should be used in the 3D search.

We, then, performed a 3D search based on Equation 4 around the point (N_3', $N_5^{(2)}$, $N_6^{(2)}$) allowing the deformation along the third, fifth and sixth normal modes. The fitting score of the best-fitting structure $\mathbf{r}(N_3^{(3)}, N_5^{(3)}, N_6^{(3)})$ for each of the 42 EM structures is listed in Table 1 as the final score. The positions ($N_3^{(3)}$, $N_5^{(3)}$, $N_6^{(3)}$) of the best-fitting structures for the 42 EM structures are shown in Figure 6. Figures 6A and 6B are the projections of the structures on the planes defined by fifth and sixth modes, and third and sixth modes, respectively.

In the 3D space, most of the best-fitting structures were distributed close to a single straight line, which is shown by a black dotted line in Figure 6. Of the 42 best-fitting structures, 25 were within the distance of 5 from the line, and 37 within 10, which roughly corresponds to 0.5 and 1.0 Å in rmsd, respectively. This distribution suggests that there is a specific pathway for a large conformational change.

From Figure 6B, it is clear that the third and sixth modes were negatively correlated. That is, the best-fitting structure with a small $N_3^{(3)}$ value tended to have a large $N_6^{(3)}$ value. In the third mode, the motion of the L1 stalk was dominant as is shown in Figure 3A. When $N_3^{(3)}$ increased, the L1 stalk lifted up. It has been shown that the L1 stalk interacts with the tRNA molecule at the E site (E-tRNA), and this interaction blocks the exit path

for the E-tRNA and, thus, it has been suggested that the movement of the L1 stalk is necessary for the release of the E-tRNA (Yusupov et al., 2001). The best-fitting structures with positive $N_3^{(3)}$ values had the L1 stalk in the nonblocking state, and those with negative values had the L1 stalk in the blocking state. Thus, the correlation between the third and sixth modes indicates that the best-fitting structures with a large distortion along the positive direction of the ratchet-like mode (Figure 3C) tended to have the L1 stalk in the blocking state. Valle et al. (2003c) have already suggested that the motion of the L1 stalk correlates with the ratchet-like motion. Although their observation came from a study of EFG bound structures, Figure 6B shows that this is generally the case.

There were some exceptions to this, such as EMD-1064, -1071, and -1110. In EMD-1064 and -1071, although the L1 stalk was in a blocking state (negative $N_3^{(3)}$), ratchet-like deformation was small (small $N_6^{(3)}$). This may be due to the quality of the EM density maps. As shown in Figure 3A, the motion in the third mode was more localized than in the fifth and sixth modes. Thus, the quality of the EM density maps could be more influential on the fitting score. Indeed, the resolution of EMD-1064 is low, compared with that of the others (Table 1). In the EM-density map of EMD-1071, the L1 stalk site is not well defined, and thus the position of the best-fitting structure along the third mode is not reliable. In the case of EMD-1110, the situation was different. Although a large ratchet-like deformation was observed, the L1 stalk was not in a blocking state. This is probably because this structure does not have E-tRNA. Thus, this suggests that the blocking state of the L1 stalk is stabilized by the interaction with the E-tRNA.

Most of the best-fitting structures with small $N_6^{(3)}$ values ($N_6^{(3)} \leq 20$) were distributed in a small area, which can be seen clearly in Figure 6A. This suggests that these EM structures were in states around a stable "ground state" of the 70S ribosome. The position of the PDB structure (0,0,0) is outside of this distribution, suggesting again that the PDB structure is fairly distorted.

Other structures with larger $N_6^{(3)}$ values (shown in Figure 6) were distributed widely along the third and the sixth modes. They are the structures for an initiation complex (EMD-1248) and complexes bound with EFG (EMD-1110, -1315, -1363, and -1365), RF3 (EMD-1065 and -1302), RRF (EMD-1128 and -1370), and SecYEG (EMD-1143). Except for EMD-1110 and -1143, it has already been suggested that these structures may represent structures in which the ratchet-like conformational change has already occurred (Allen et al., 2005; Gao et al., 2005, 2007; Klaholz et al., 2004; Connell et al., 2007; Valle et al., 2003c; Barat et al., 2007). However, as far as we know, this is the first time that many EM structures have been compared quantitatively. The best-fitting structures for these EM structures, whose ratchet-like conformational changes have been reported, had $N_6^{(3)}$ values larger than or equal to 25. Thus, it would be reasonable if the structures with such $N_6^{(3)}$ values are the ones in which the ratchet-like conformational change has occurred. By this criterion, EMD-1110 and -1143 are structures with ratchet-like conformational changes, although this has not been reported in the literature (Diaconu et al., 2005; Mitra et al., 2005).

The EM structures bound with these factors such as EFG did not always show large conformational changes. For example, of the six EM structures bound with EFG (red circles in Figure 6), two structures (EMD-1362 and -1366) had small $N_6^{(3)}$ values. However, very interestingly, except for EMD-1110, the best-fitting structures for EFG-bound EM structures were distributed close to the dotted straight red line in Figure 6 (the maximum distance is less than 4 in 3D space). This suggests that the 70S ribosome bound with EFG changes its conformation along a specific pathway in a concerted manner. Similarly, three EM structures bound with RRF (EMD-1077, -1128, and -1370 shown by green circles in Figure 6) were distributed close to a dotted straight green line (the maximum distance is less than 3 in 3D space).

Another interesting point is that the best-fitting structures with the largest ratchet-like deformations among the 42 structures were distributed in a small area, suggesting that they were similar to each other. They are the structures for EMD-1065, -1128, -1315, and -1363 (because of the low resolution and the low fitting score, the position of the best-fitting structure for EMD-1065 is not certain). This result may suggest that these EM structures have the maximum ratchet-like conformational change which the 70S ribosome can make. The reason is as follows: as $N_3^{(3)}$ decreases, the L1 stalk approaches the E-tRNA. Thus, there should be a lower limit for $N_3^{(3)}$. Otherwise, the L1 stalk would clash with the E-tRNA. On the other hand, because the third and the sixth modes are negatively correlated, $N_6^{(3)}$ should have an upper limit—that is, there is a maximum for the ratchet-like conformational change. It could be possible that these four EM structures happened to have similar structures. However, considering that these EM structures have different bound molecules (RF3 for EMD-1065, EF-G for EMD-1315 and -1363, and RRF for EMD-1128) and have been obtained by different groups, it seems more probable that they are all structures with the maximum ratchet-like conformational change that the 70S ribosome can make.

Conclusion

We analyzed EM structures of 70S ribosome by using normal mode analysis and a new fitting technique. The normal mode analyses of the elastic network model were performed to build a few series of deformed atomic structures along each of a few lowest frequency modes of the PDB structure. Large deformation of the atomic structure was achieved by performing normal mode analysis iteratively. The library of ready-made deformed atomic structures was built from these series of structures based on Equation 2.

We first performed a 1D search, in which each series of deformed atomic structures was fitted into each EM structure, and the best-fitting atomic structure—namely, the one with the highest fitting score in each series—was identified. This search was performed to see which normal modes should be used in Equation 2. From the increase in the fitting score, we found that the fifth and sixth modes were the most effective in improving the fitting, followed by the third mode.

Then we performed a 2D search by combining the fifth and sixth modes. The 2D search was performed to quickly obtain the best-fitting structure at the next stage (3D search), or to reduce the computational time in the 3D search. This search may not be necessary when we study smaller structures, which require fewer computational resources.

Finally, we performed a 3D search by combining the third, fifth and sixth modes. The analysis showed that the third and sixth modes were negatively correlated—that is, the EM structures with large deformations along the positive direction of the sixth mode (ratchet-like conformational change) tended to be

deformed along the negative direction of the third mode. In the third mode, the motions of the L1 stalk were dominant. Thus, this result showed the ratchet-like motions and the motions of the L1 stalk occurred simultaneously.

The most interesting result in this study was that the EM structures bound with EFG or RRF were aligned along the same straight line in the conformational space (Figure 6), although they distributed quite widely in the space, especially along the directions of the third and sixth modes. The result suggests that the 70S ribosome bound with these factors changes its conformation along a specific pathway in a concerted manner.

The advantage of our approach to analyzing EM structures is that once the library of deformed structures has been built, the analysis of newly determined EM structures is fast and comparing the new structures with previously analyzed structures is straightforward.

EXPERIMENTAL PROCEDURES

Building EM Structures from 3D-EM Maps

As of September 2008, 44 3D-EM maps of the 70S ribosome were available in EMDB at EBI (http://www.ebi.ac.uk/pdbe/emdb/). We used all these maps in our calculations (Table 1). In the 3D-EM maps, the EM density ρ is given for each voxel, which occupies a space (x, y, z), where $i_x\, p \le x < (i_x + 1)\, p$, $i_y\, p \le y < (i_y + 1)\, p$, $i_z\, p \le z < (i_z + 1)\, p$, and i_x, i_y, and i_z are integers, and p is the voxel size given for each 3D-EM map. From each 3D-EM map, we built an EM structure as follows. We defined that each EM structure was composed of voxels whose density ρ was higher than a threshold value ρ_0. The threshold value ρ_0 was determined so that the volume occupied by the EM structure ($= N_v p^3$, where N_v is the number of voxels with a density higher than ρ_0) was equivalent to the molecular volume of the PDB structure of the 70S ribosome calculated by a program VOIDOO (Kleywegt et al., 2001; Kleywegt and Jones, 1993, 1994), in which the probe radius was set to 1.4 Å. EMD-1143 includes a large extra particle (protein conducting channel), so we increased the volume of the EM structure by about 10%, compared with the other structures. Note that we added hydrogen atoms and missing residues (Ishida and Hayward, 2008) to the original PDB structure (PDBID: 1YL3 and 1YL4; Jenner et al., 2005) and removed tRNAs and mRNA. In this article, we call this modified PDB structure the PDB structure.

Elastic Network Model of Ribosome

Ribosome is a huge molecular complex, and the PDB structure is composed of more than 250,000 atoms including hydrogens. We used an elastic network model because it would require a lot of computational resources to deform such a huge structure if an all-atom model is used. The elastic network model is based on atomic positions and cutoff distances. Ribosome consists of amino-acid and nucleotide chains. In our elastic network model, each amino-acid residue was represented by a Cα atom, and each nucleotide residue was represented by a P atom—that is, the position of each residue was described by that of either of these atoms, and the total mass of each residue was put on either of these atoms. Each pair of residues was connected by a spring with a spring constant C if they were within cutoff distance R_C. Following the approach used by Tama et al. (2003), we used different cutoff distances for different pairs of residues—that is, R_C = 20 Å for pairs of N–N and N–A and R_C = 16 Å for A–A, where N and A refer to nucleic-acid and amino-acid residues, respectively.

Iterative Normal Mode Calculation

In this study, the elastic network model of the 70S ribosome was deformed along its normal modes. If we describe the elastic network model of the nondeformed PDB structure by a $3N_r$-dimensional vector $\mathbf{r}_0$, where N_r is the total number of residues, the deformed structure $\mathbf{r}_1^k$ is described as $\mathbf{r}_0 + \alpha \mathbf{v}_0^k$, where $\mathbf{v}_0^k$ is a normalized k th lowest frequency normal mode vector ($|\mathbf{v}_0^k| = 1$) obtained for the structure $\mathbf{r}_0$ and α determines how far the structure is deformed. By this deformation, each residue is moved linearly in the direction of the normal mode vector. However, large linear movements destroy the structure; thus, to maintain the structure stereochemically, only a small deformation is allowed.

Normal mode analysis can be performed on the energy minimized structure. Thus, in the conventional approach, time-consuming energy minimization is necessary. On the other hand, in the elastic network model, the energy function is defined in such a way that the given structure is in the energy minimized state. Thus, normal mode calculation can be applied to any given conformation (Miyashita et al., 2003). We applied the calculation to the slightly deformed structure $\mathbf{r}_1^k$ and obtained the normal mode vectors. Among them, the most similar normal mode vector $\mathbf{v}_1^{k_1}$ to $\mathbf{v}_0^k$ ($\mathbf{v}_0^k \cdot \mathbf{v}_1^{k_1} \sim 1$) was used to build the next structure $\mathbf{r}_2^k$ ($= \mathbf{r}_1^k + \alpha \mathbf{v}_1^{k_1}$). Note that k_1 is not always equal to k, because the order of the normal modes could be different for the deformed structure. The calculation was repeated, and a series of structures $\{\mathbf{r}_n^k; n = 1, \ldots, n_+\}$, where $\mathbf{r}_n^k = \mathbf{r}_0 + \alpha \mathbf{v}_0^k + \alpha \mathbf{v}_1^{k_1} + \alpha \mathbf{v}_2^{k_2} + \ldots + \alpha \mathbf{v}_{(n-1)}^{k_{(n-1)}}$, was obtained. Another series of structures was built for the opposite direction—that is, starting from the initial structure $\mathbf{r}_0$, a deformed structure $\mathbf{r}_{-1}^k (= \mathbf{r}_0 - \alpha \mathbf{v}_0^k)$ was built. The calculation was repeated and another series of structures $\{\mathbf{r}_{-n}^k; n = 1, \ldots, n_-\}$ was obtained. We refer to these two series of structures ($\mathbf{r}_n^k$ and $\mathbf{r}_{-n}^k$) as deformed structures along the k th normal mode. In this study, we set the value of the parameter α to 0.1, which means that the rmsd between $\mathbf{r}_{n-1}^k$ and $\mathbf{r}_n^k$, where n runs from $(-n_- + 1)$ to n_+ and $\mathbf{r}_0^k = \mathbf{r}_0$, was 0.1 Å.

Building an All-Atom Model from an Elastic Network Model

Our analysis of the EM structures was performed by looking for the atomic structure that best-fitted into each EM structure. We used an all-atom model for the atomic structure in the fitting procedure. However, each residue of the elastic network model was represented by a single point, which corresponded to a P or Cα atom. Thus, we needed to reconstruct the all-atom model from the deformed elastic network model. We determined these positions as follows. We assumed that each residue in the PDB structure was a rigid body and applied a rotational and translational manipulation to it. This manipulation best-fits the representative atoms (the P and Cα atoms) in the residue and the nearby residues in the PDB structure to the corresponding points in the deformed elastic network model through a least-square fitting procedure. In this way, the positions of the atoms in the deformed structure were obtained.

Fitting Each Atomic Structure into Each EM Structure

Each atomic structure of the 70S ribosome was fitted as a rigid body into each EM structure by rotational and translational manipulations to maximize the scoring function. We defined the scoring function as a ratio of the number of atoms inside the space occupied by the EM structure to the total number of atoms. This simple scoring function was used for the fast calculations. The computational detail of the fitting will be published elsewhere.

SUPPLEMENTAL DATA

Supplemental Data include two tables, three movies, and Supplemental Experimental Procedures and can be found with this article online at http://www.cell.com/structure/supplemental/S0969-2126(09)00418-3.

ACKNOWLEDGMENTS

We thank Yvonne Ishida for reading this manuscript carefully. This work was supported by Strategic International Cooperation Program and Core Research for Evolutional Science and Technology (CREST), Japan Science and Technology Agency and by Grants-in-Aid for Scientific Research on Priority Areas (No. 17053029) from the Ministry of Education, Culture, Sports, Science and Technology of Japan.

Received: May 22, 2009
Revised: September 25, 2009
Accepted: September 27, 2009
Published: December 8, 2009

REFERENCES

Agrawal, R.K., Sharma, M.R., Kiel, M.C., Hirokawa, G., Booth, T.M., Spahn, C.M., Grassucci, R.A., Kaji, A., and Frank, J. (2004). Visualization of ribosome-recycling factor on the *Escherichia coli* 70s ribosome: functional implications. Proc. Natl. Acad. Sci. USA *101*, 8900–8905.

Allen, G.S., Zavialov, A., Gursky, R., Ehrenberg, M., and Frank, J. (2005). The cryo-EM structure of a translation initiation complex from *Escherichia coli*. Cell *121*, 703–712.

Barat, C., Datta, P.P., Raj, V.S., Sharma, M.R., Kaji, H., Kaji, A., and Agrawal, R.K. (2007). Progression of the ribosome recycling factor through the ribosome dissociates the two ribosomal subunits. Mol. Cell *27*, 250–261.

Connell, S.R., Takemoto, C., Wilson, D.N., Wang, H., Murayama, K., Terada, T., Shirouzu, M., Rost, M., Schuler, M., Giesebrecht, J., et al. (2007). Structural basis for interaction of the ribosome with the switch regions of GTP-bound elongation factors. Mol. Cell *25*, 751–764.

Diaconu, M., Kothe, U., Schlunzen, F., Fischer, N., Harms, J.M., Tonevitsky, A.G., Stark, H., Rodnina, M.V., and Wahl, M.C. (2005). Structural basis for the function of the ribosomal l7/12 stalk in. Cell *121*, 991–1004.

Frank, J. (1996). Three-Dimensional Electron Microscopy of Macromolecular Assemblies (San Diego, CA: Academic Press).

Frank, J., and Agrawal, R.K. (2000). A ratchet-like inter-subunit reorganization of the ribosome during translocation. Nature *406*, 318–322.

Gabashvili, I.S., Agrawal, R.K., Spahn, C.M., Grassucci, R.A., Svergun, D.I., Frank, J., and Penczek, P. (2000). Solution structure of the *E. coli* 70s ribosome at 11.5 Å resolution. Cell *100*, 537–549.

Gao, N., Zavialov, A.V., Li, W., Sengupta, J., Valle, M., Gursky, R.P., Ehrenberg, M., and Frank, J. (2005). Mechanism for the disassembly of the posttermination complex inferred from cryo-EM studies. Mol. Cell *18*, 663–674.

Gao, H., Zhou, Z., Rawat, U., Huang, C., Bouakaz, L., Wang, C., Cheng, Z., Liu, Y., Zavialov, A., Gursky, R., et al. (2007). RF3 induces ribosomal conformational changes responsible for dissociation of class I release factors. Cell *129*, 929–941.

Gilbert, R.J., Fucini, P., Connell, S., Fuller, S.D., Nierhaus, K.H., Robinson, C.V., Dobson, C.M., and Stuart, D.I. (2004). Three-dimensional structures of translating ribosomes by cryo-EM. Mol. Cell *14*, 57–66.

Gillet, R., Kaur, S., Li, W., Hallier, M., Felden, B., and Frank, J. (2007). Scaffolding as an organizing principle in trans-translation. The roles of small protein b and ribosomal protein s1. J. Biol. Chem. *282*, 6356–6363.

Halic, M., Blau, M., Becker, T., Mielke, T., Pool, M.R., Wild, K., Sinning, I., and Beckmann, R. (2006). Following the signal sequence from ribosomal tunnel exit to signal recognition particle. Nature *444*, 507–511.

Humphrey, W., Dalke, A., and Schulten, K. (1996). VMD—Visual Molecular Dynamics. J. Mol. Graph. *14*, 33–38.

Ishida, H., and Hayward, S. (2008). Path of nascent polypeptide in exit tunnel revealed by molecular dynamics simulation of ribosome. Biophys. J. *95*, 5962–5973.

Jenner, L., Romby, P., Rees, B., Schulze-Briese, C., Springer, M., Ehresmann, C., Ehresmann, B., Moras, D., Yusupova, G., and Yusupov, M. (2005). Translational operator of mRNA on the ribosome: how repressor proteins exclude ribosome binding. Science *308*, 120–123.

Kaur, S., Gillet, R., Li, W., Gursky, R., and Frank, J. (2006). Cryo-EM visualization of transfer messenger RNA with two smpbs in a stalled ribosome. Proc. Natl. Acad. Sci. USA *103*, 16484–16489.

Klaholz, B.P., Pape, T., Zavialov, A.V., Myasnikov, A.G., Orlova, E.V., Vestergaard, B., Ehrenberg, M., and van Heel, M. (2003). Structure of the *Escherichia coli* ribosomal termination complex with release factor 2. Nature *421*, 90–94.

Klaholz, B.P., Myasnikov, A.G., and Van Heel, M. (2004). Visualization of release factor 3 on the ribosome during termination of protein synthesis. Nature *427*, 862–865.

Kleywegt, G., Zou, J., Kjeldgaard, M., and Jones, T. (2001). Around O. In International Tables for Crystallography, Vol. F. Crystallography of Biological Macromolecules, M. Rossmann and E. Arnold, eds. (Dordrecht, The Netherlands: Kluwer Academic Publishers), pp. 353–356, 366–367.

Kleywegt, G.J., and Jones, T.A. (1994). Detection, delineation, measurement and display of cavities in macromolecular structures. Acta Crystallogr. D Biol. Crystallogr. *50*, 178–185.

Kleywegt, G.J., and Jones, T. (1993). Biomacromolecular speleology. CCP4/ESF-EACBM Newsletter on Protein Crystallography *29*, 26–28.

Konevega, A.L., Fischer, N., Semenkov, Y.P., Stark, H., Wintermeyer, W., and Rodnina, M.V. (2007). Spontaneous reverse movement of mRNA-bound tRNA through the ribosome. Nat. Struct. Mol. Biol. *14*, 318–324.

Marzi, S., Myasnikov, A.G., Serganov, A., Ehresmann, C., Romby, P., Yusupov, M., and Klaholz, B.P. (2007). Structured mRNAs regulate translation initiation by binding to the platform of the ribosome. Cell *130*, 1019–1031.

Matsumoto, A., and Olson, W.K. (2002). Sequence-dependent motions of DNA: A normal mode analysis at the base-pair level. Biophys. J. *83*, 22–41.

Mitra, K., Schaffitzel, C., Shaikh, T., Tama, F., Jenni, S., Brooks, C.L., 3rd, Ban, N., and Frank, J. (2005). Structure of the *E. coli* protein-conducting channel bound to a translating ribosome. Nature *438*, 318–324.

Miyashita, O., Onuchic, J.N., and Wolynes, P.G. (2003). Nonlinear elasticity, proteinquakes, and the energy landscapes of functional transitions in proteins. Proc. Natl. Acad. Sci. USA *100*, 12570–12575.

Myasnikov, A.G., Marzi, S., Simonetti, A., Giuliodori, A.M., Gualerzi, C.O., Yusupova, G., Yusupov, M., and Klaholz, B.P. (2005). Conformational transition of initiation factor 2 from the GTP- to GTP-bound state visualized on the ribosome. Nat. Struct. Mol. Biol. *12*, 1145–1149.

Poornam, G.P., Matsumoto, A., Ishida, H., and Hayward, S. (2009). A method for the analysis of domain movements in large biomolecular complexes. Proteins *76*, 201–212.

Rawat, U.B., Zavialov, A.V., Sengupta, J., Valle, M., Grassucci, R.A., Linde, J., Vestergaard, B., Ehrenberg, M., and Frank, J. (2003). A cryo-electron microscopic study of ribosome-bound termination factor RF2. Nature *421*, 87–90.

Rawat, U., Gao, H., Zavialov, A., Gursky, R., Ehrenberg, M., and Frank, J. (2006). Interactions of the release factor RF1 with the ribosome as revealed by cryo-EM. J. Mol. Biol. *357*, 1144–1153.

Schaffitzel, C., Oswald, M., Berger, I., Ishikawa, T., Abrahams, J.P., Koerten, H.K., Koning, R.I., and Ban, N. (2006). Structure of the *E. coli* signal recognition particle bound to a translating ribosome. Nature *444*, 503–506.

Stark, H., Rodnina, M.V., Wieden, H.J., Zemlin, F., Wintermeyer, W., and van Heel, M. (2002). Ribosome interactions of aminoacyl-tRNA and elongation factor Tu in the codon-recognition complex. Nat. Struct. Biol. *9*, 849–854.

Tama, F., Valle, M., Frank, J., and Brooks, C.L., 3rd. (2003). Dynamic reorganization of the functionally active ribosome explored by normal mode analysis and cryo-electron microscopy. Proc. Natl. Acad. Sci. USA *100*, 9319–9323.

Tama, F., Miyashita, O., and Brooks, C.L., 3rd. (2004a). Flexible multi-scale fitting of atomic structures into low-resolution electron density maps with elastic network normal mode analysis. J. Mol. Biol. *337*, 985–999.

Tama, F., Miyashita, O., and Brooks, C.L., 3rd. (2004b). Normal mode based flexible fitting of high-resolution structure into low-resolution experimental data from cryo-EM. J. Struct. Biol. *147*, 315–326.

Trabuco, L.G., Villa, E., Mitra, K., Frank, J., and Schulten, K. (2008). Flexible fitting of atomic structures into electron microscopy maps using molecular dynamics. Structure *16*, 673–683.

Valle, M., Sengupta, J., Swami, N.K., Grassucci, R.A., Burkhardt, N., Nierhaus, K.H., Agrawal, R.K., and Frank, J. (2002). Cryo-EM reveals an active role for aminoacyl-tRNA in the accommodation process. EMBO J. *21*, 3557–3567.

Valle, M., Gillet, R., Kaur, S., Henne, A., Ramakrishnan, V., and Frank, J. (2003a). Visualizing tmRNA entry into a stalled ribosome. Science *300*, 127–130.

Valle, M., Zavialov, A., Li, W., Stagg, S.M., Sengupta, J., Nielsen, R.C., Nissen, P., Harvey, S.C., Ehrenberg, M., and Frank, J. (2003b). Incorporation of aminoacyl-tRNA into the ribosome as seen by cryo-electron microscopy. Nat. Struct. Biol. *10*, 899–906.

Valle, M., Zavialov, A., Sengupta, J., Rawat, U., Ehrenberg, M., and Frank, J. (2003c). Locking and unlocking of ribosomal motions. Cell *114*, 123–134.

Wang, Y., Rader, A.J., Bahar, I., and Jernigan, R.L. (2004). Global ribosome motions revealed with elastic network model. J. Struct. Biol. *147*, 302–314.

Yusupov, M.M., Yusupova, G.Z., Baucom, A., Lieberman, K., Earnest, T.N., Cate, J.H., and Noller, H.F. (2001). Crystal structure of the ribosome at 5.5 Å resolution. Science *292*, 883–896.